Evaluation of a Kalman-based block matching method to assess the bi-dimensional motion of the carotid artery wall in B-mode ultrasound sequences

Guillaume Zahnd[a,*], Maciej Orkisz[a], André Sérusclat[b], Philippe Moulin[c,d], Didier Vray[a]

[a] *Université de Lyon, CREATIS; CNRS UMR 5220; INSERM U1044; INSA-Lyon; Université Lyon 1, France*
[b] *Department of Radiology, Louis Pradel Hospital, Lyon, France*
[c] *Department of Endocrinology, Louis Pradel Hospital; Hospices Civils de Lyon; Université Lyon 1, Lyon, France*
[d] *INSERM UMR 1060, Lyon, France*

Medical Image Analysis, 17(5), 573–585, 2013
Final version available at:
http://www.medicalimageanalysisjournal.com/article/S1361-8415%2813%2900036-4/fulltext

Abstract

We aim at investigating arterial diseases at early stage, by assessing the longitudinal (*i.e.* in the same direction as the blood flow) motion of the intima-media complex. This recently evidenced phenomenon has been shown to provide relevant and complementary information about vascular health.

Our method assesses the longitudinal and radial motion from clinical *in vivo* B-mode ultrasound sequences. To estimate the trajectory of a selected point during the cardiac cycle, we introduce a block matching method that involves a temporal update of the reference block using a pixel-wise Kalman filter. The filter uses the initial gray-level of the pixel as control signal to avoid divergence due to cumulating errors. The block and search-window sizes are adapted to the tissue of interest.

The method was evaluated on image sequences of the common carotid artery, acquired in 57 healthy volunteers and in 25 patients at high cardiovascular risk.

*Corresponding author
E-mail: guillaume.zahnd@creatis.insa-lyon.fr
Address: Creatis - INSA Lyon, Bât. Blaise Pascal, 7 Av. Jean Capelle, 69100 Villeurbanne, France
Telephone: +33 4 72 43 87 86

Reference trajectories were generated for each sequence by averaging the tracings performed by three observers. Six different computerized techniques were also compared to our method.

With a pixel size of $30\,\mu$m, the average absolute motion estimation errors were $84 \pm 107\,\mu$m and $20 \pm 19\,\mu$m for the longitudinal and radial directions, respectively. This accuracy was of the same order of magnitude as the inter- and intra-observers variability, and smaller than for the other methods. The estimated longitudinal motion amplitude was significantly reduced in at-risk patients compared with healthy volunteers ($408 \pm 281\,\mu$m *vs* $643 \pm 274\,\mu$m, $p < 0.0001$).

Our method can constitute a reliable and time-saving technique to investigate the arterial stiffness in clinical studies, in the objective to detect early-stage atherosclerosis.

Keywords: Carotid artery, Atherosclerosis, Speckle tracking, Block matching, Kalman filter, Longitudinal Motion, Cardiovascular Risk Marker

---

1. Introduction

1.1. Clinical context

Cardiovascular diseases represent the major cause of morbidity and mortality in middle- and high-income countries (WHO, 2011). Atherosclerosis, a syndrome affecting arterial blood vessels, is characterized by arterial wall stiffening and thickening, and potentially leads to thrombosis or stroke (Laurent et al., 2001). The common carotid artery (CCA, Fig. 1) being principally affected by this disease, it is widely considered for screening at early stage, that is to say before anatomical alteration such as the formation of atheromatous plaques (Gamble et al., 1994). The CCA consists of three concentric layers (*i.e.* intima, media and adventitia) around the lumen where the blood flows from the heart to the brain (Fig. 1).

Traditional risk markers focus on the two innermost layers thickening and stiffening. Carotid intima-media thickness (IMT) and its variation have been shown to have prognostic value for cardiac infarction and were also strictly correlated to the presence of coronary artery disease (Mutlu et al., 2011). Pulse wave velocity (PWV) was also demonstrated to represent an independent predictor of all-cause and cardiovascular mortality (Laurent et al., 2001). Arterial distensibility (*i.e.* cross-sectional diameter change) has been shown to be associated to cardiovascular risk in patients who already have vascular disease or atherosclerotic risk factors (Simons et al., 1999). However, the performance of these traditional risk markers as screening tests for subclinical atherosclerosis remains relatively poor (Simon et al., 2006).

On the other hand, the characterization of the arterial wall dynamics in the longitudinal plane, *i.e.* in the same axial direction as the blood flow, has only been little studied, although it is likely to further characterize the arterial compliance and may provide relevant and complementary clinical information about vascular health. Indeed, recent clinical investigations showed that the wall longitudinal motion was a predictor for cardiovascular accidents (Svedlund et al., 2011), was associated with the presence of cardiovascular risk factors (Ahlgren et al., 2009, 2012; Zahnd et al., 2011a), and was independent of established traditional risk markers while demonstrating a better screening potential (Zahnd et al., 2012).

As opposed to the radial motion (*i.e.* along the same direction as the cross-sectional diameter), the longitudinal motion remains more challenging to observe due to the homogeneity of the tissue layers in this direction (Fig. 1). The advances in the development of modern ultrasound (US) scanners have only recently lead to confirm the presence of the arterial longitudinal movement in an *in vivo* study (Persson et al., 2003). Please note that all along this article we use the term "longitudinal" to denote the direction of the blood flow, which is more or less horizontal in the images we

are dealing with, and the term "radial" to denote the direction perpendicular to the blood flow (vertical). This vocabulary differs from the terms usually used in the US imaging community, where "longitudinal" denotes the direction of the US propagation, *i.e.* vertical the in B-mode images.

The objective of the present work is twofold. First, we introduce a novel tracking method, dedicated to assess *in vivo* the cyclic longitudinal motion of the intima-media complex, in US B-mode image sequences of the CCA acquired in clinical practice. Second, we evaluate the accuracy of our method, and we present a comparison with existing methods.

1.2. Motion tracking in ultrasound image sequences of the CCA

Bi-dimensional (2D, *i.e.* radial and longitudinal) motion estimation in US B-mode image sequences can be assessed with a speckle tracking approach (Ophir et al., 1991). This technique consists in estimating the displacement of an echo scatterer, corresponding to a specific gray-level pattern, through the sequence.

1.2.1. General principle of the block matching technique

The speckle tracking is generally based on a block matching (BM, Fig. 2) framework (Bohs and Trahey, 1991), in which the pattern to be tracked is represented by a reference block $\mathcal{B}_{ref}$, *i.e.* a small image region encompassing the pattern. Given a specified similarity criterion, the location of the pattern in the considered frame is determined by seeking the best match between the reference block and candidate blocks within a search window. The search window is usually defined by a maximum displacement (margin) around the center $\mathbf{p}$ of the best-matched block in the previously considered frame (Fig. 2). The motion of the pattern between two consecutive frames is defined by the estimated displacement $\hat{\mathbf{d}}$ of the point $\mathbf{p}$, and the whole trajectory through the sequence is calculated by summing up all the successively estimated displacements.

1.2.2. Challenges related to the tracking of the arterial wall longitudinal motion

In our specific context, the *in vivo* estimation of the CCA wall longitudinal motion along several cardiac cycles in US B-mode imaging is hampered by three main difficulties.

First, the tracked pattern, corresponding to the texture of the considered tissues, presents a rather homogeneous profile in the longitudinal direction, with only a small variation of the image gray level along the wall. This lack of contrast is caused by the geometry of the anatomical structure of the vessel, consisting of layers aligned along the longitudinal axis (Fig. 1). Moreover, the resolution cell of the ultrasound

scanner, corresponding to the spatial definition of the image, is generally coarser in the direction perpendicular to the ultrasound beam than in the direction of the beam propagation. This is due to the shape of the scanner's point spread function (PSF): its width, determined by the probe geometry as well as by the depth of the focal zone, is most often larger than its height, determined by the ultrasound signal wavelength. These two issues lead to the aperture problem, *i.e.* there is little evidence of the longitudinal component of the motion.

Second, the small thickness of the region of interest, *i.e.* the IMT corresponding roughly to half a millimeter, also represents a challenge. Indeed, while the tracked block has to encompass a pattern sufficiently large to be discriminant, it should not include the neighboring regions, lumen and adventitia, which have significantly different characteristics. In particular, whereas adventitia is almost still, the blood flow within the lumen is much faster than the intima-media motion to be estimated.

Third, the issue of speckle decorrelation, *i.e.* the degrading phenomenon caused by out-of-plane movements, low echoes, tissue deformation and movement artifacts, often leads to modifications of the tracked speckle pattern during the sequence. Moreover, the imaging quality corresponding to clinical routine can vary greatly between different subjects, mostly due to the variability of the tissue echogenicity, and can introduce blur or high noise. This issue, inherent to clinical US B-mode imaging, indeed represents a potential source of error for speckle tracking techniques, as it may provoke a divergence in the trajectory estimation due to successive error cumulation.

1.2.3. Previous work related to the wall longitudinal motion

Recent work has contributed to characterize *in vivo* the specific longitudinal motion of the human CCA wall in US B-mode image sequences, using different speckle tracking approaches.

A first study (Golemati et al., 2003) used a traditional BM technique, with block and window of dimensions, respectively, $3.20 \times 2.50\,\mathrm{mm}^2$ and $4.50 \times 3.80\,\mathrm{mm}^2$ (*i.e.* margin 0.65 mm in both directions). This approach therefore considered a wide region in the image, permitting *i)* to include a texture presenting a more contrasted pattern in the longitudinal direction, and *ii)* to increase the robustness to the speckle decorrelation issue. However the dimensions of the block were large in comparison with the considered tissue thickness, possibly leading to a loss of precision. Indeed, the investigated region, centered on the intima-media complex, also covered part of the lumen and the adventitia tissues.

Another team proposed a different technique based on echo tracking (Persson et al., 2003; Cinthio et al., 2005, 2006), focusing on a very local region of the image with smaller block and window dimensions, respectively, $0.10 \times 0.10\,\mathrm{mm}^2$ and $0.70 \times$

$0.70\,\mathrm{mm}^2$ (*i.e.* margin 0.30 mm in both directions). This approach also addressed the issue of the lack of contrast of the longitudinal profile by tracking a single well distinguishable scatter. Experimental *in vivo* trials showed high tracking accuracy, and permitted a detailed analysis of the arterial longitudinal motion during the cardiac cycle. From our experience however, such a small block size is sensitive to noise, and would therefore not be well suited to clinical routine and large population studies, where image quality varies from one subject to another.

Our team recently proposed a different approach, denoted as Multi-Block Matching (MBM) (Zahnd et al., 2011a, 2012), aiming to assess the global motion of the wall over a wide region of the intima-media complex by tracking multiple longitudinally aligned points. The rationale of this framework is the following. First, the speckle decorrelation issue is addressed by an Eulerian block matching approach. This strategy involves an automatic and regular re-positioning of the blocks within the intima-media complex in each frame of the image, using the *a priori* information provided by the segmentation of the interfaces. In such manner, the drifting issue that can occur when the tracked pattern is altered during the sequence is avoided, as the motion of the tissues is assessed through a fixed window. Second, a series of 16 blocks is used to estimate the global motion of the entire length of the wall, in order to increase the robustness of the method. Indeed, as some regions of the image can temporarily suffer from noise during the sequence, the motion is assessed independently by a block matching technique at regular position interval, and the final resulting motion is determined by the median value of all estimates. Third, the dimension of the blocks and windows, respectively, $1.50 \times 0.30\,\mathrm{mm}^2$ and $2.10 \times 0.90\,\mathrm{mm}^2$ (*i.e.* margin 0.30 mm in both directions), aims to fit the morphology of the arterial wall layers. This approach however may underestimate the amplitude of the actual motion, as the median operation that is performed does not favor the displacement values that are maximal.

A recent study (Gastounioti et al., 2011) introduced a more robust speckle tracking scheme, in order to cope with the issue of speckle decorrelation by exploiting a Kalman filtering approach (Kalman, 1960; Welch and Bishop, 1995). The block and window dimensions used in that study were, respectively, $1.60 \times 1.00\,\mathrm{mm}^2$ and $2.90 \times 2.30\,\mathrm{mm}^2$ (*i.e.* margin 0.65 mm in both directions). This promising work showed that the use of Kalman filtering as an adaptive strategy to update either the reference block or the 2D trajectory position permits to decrease the estimation error generated by classical speckle tracking methods. However, the proposed approach performs a scheme estimation *via* a fading memory system that does not involve a control signal. Therefore, the divergence issue due to successive error cumulation during the sequence remains as a potential source of error.

It is also noteworthy to mention that a different team recently proposed to use the Velocity Vector Imaging commercial software (VVI, Research Arena 2; TomTec imaging systems GmbH, Unterschleissheim, Germany), in order to investigate the longitudinal motion amplitude of the carotid artery wall in several clinical studies (Svedlund and Gan, 2011; Svedlund et al., 2011).

1.3. Objective and summary of the proposed approach

Our work focuses on estimating the 2D trajectories (both the longitudinal and radial components) representing the intima-media complex motion during the cardiac cycle in US B-mode image sequences. The objective was to develop a method capable of processing the sequences acquired in clinical practice as accurately as human experts, while requiring significantly less effort and remaining more reproducible. The goal of this article is to describe the developed method and to evaluate it by comparing it with both reference trajectories traced by experts and with other methods.

Our method is based on a Kalman-filtering scheme that performs the update of the tracked reference pattern during the sequence, in the objective to cope with speckle decorrelation issues. Namely, the Kalman filter estimates the gray levels of the reference block $\mathcal{B}_{ref}$ used within the speckle tracking framework. The main originality of our approach resides in the use of a control signal, corresponding to the initial state of the system $\mathcal{B}_{ref}(1)$, expected to avoid the divergence of the trajectory across the cyclic motion of the tracked pattern. Indeed, this pattern, corresponding to a local region of the tissues in the intima-media complex, generally undergoes an alteration during the heart cycle. This alteration, due to the reasons explained in the previous section, usually increases with the distance from the initial position. As the observed motion is quasi-periodic, the region of interest is expected to periodically recover its initial appearance when getting back close to the starting point. The remaining characteristics of our method are the following. Firstly, we have chosen to update each pixel of the reference block independently, so that localized variations of intensity do not impact on the other pixels of the block. Secondly, the choice of the block and search-window size was adapted to the arterial structure of interest and to its motion. Namely, the block height and width respectively are slightly inferior to the IMT and roughly equivalent to the empirically determined typical longitudinal size of the tracked echoes, while the search window height and width were set such that the margin corresponds to the maximum possible 2D displacement between two consecutive frames.

The accuracy of our Kalman Block Matching (KBM) method was evaluated *in vivo* on the carotid distal wall of 82 subjects (57 healthy volunteers and 25 at high

cardiovascular risk patients) in US B-mode sequences. The results of our method were compared with those obtained manually by three experts, and differed from the reference not more than the experts between them, while being fully reproducible. A comparison was also carried out with six computerized methods representing the main characteristics of the published work that investigated the wall longitudinal motion. The KBM method demonstrated the highest accuracy. Finally, in the aim to confirm the clinical relevance of the wall longitudinal motion estimated with our KBM method, a comparison was performed between healthy volunteers and at-risk patients. A statistical analysis showed that the amplitude of the estimated longitudinal motion was significantly reduced in at-risk patients.

2. Material and methods

2.1. Initialization phase

In the first frame $\mathcal{I}(1)$ of the sequence, the user selects a single point $\mathbf{p}(1)$ within the intima-media complex. The region that will be tracked with our KBM method during the whole sequence is defined by a rectangular block $\mathcal{B}$ centered on the initial point, the size of which is well adapted to the wall anatomy. Preferably, the selected point $\mathbf{p}(1)$ should correspond to a well distinguishable echo, *i.e.* to a bright local scatterer contrasting with the surrounding uniform speckle texture, and is expected to remain visually perceptible during the whole sequence (Fig. 3). This initialization phase is very quick and easy, thanks to a smart implementation that allows the user to preview the whole sequence and set the position of the desired initial point.

2.2. Kalman filter

We first provide a brief description of the Kalman filter theory, in order to introduce the notations that are used in our specific implementation, which is subsequently detailed.

2.2.1. Theoretical background

In a general manner, the Kalman filter (Kalman, 1960; Welch and Bishop, 1995) provides the statistically optimal estimation $\hat{\mathbf{x}}$ of the state vector $\mathbf{x}$ in a discrete dynamic system governed by the following linear stochastic difference equation:

$$\mathbf{x}(n+1) = \mathbf{A}(n)\mathbf{x}(n) + \mathbf{B}(n)\mathbf{u}(n) + \mathbf{w}(n), \tag{1}$$

where $\mathbf{A}(n)$ is the state transition matrix, $\mathbf{B}(n)$ is the control matrix, $\mathbf{u}(n)$ is the control signal, and $\mathbf{w}(n)$ is the process noise, white, with zero mean and covariance matrix $\mathbf{Q}(n)$. It is assumed that the state $\mathbf{x}(n)$ cannot be directly assessed, instead it is measured through an observation $\mathbf{z}(n)$, defined by:

$$\mathbf{z}(n) = \mathbf{H}(n)\mathbf{x}(n) + \mathbf{v}(n), \tag{2}$$

where $\mathbf{H}(n)$ is the observation matrix and $\mathbf{v}(n)$ is the observation noise, white, with zero mean and covariance matrix $\mathbf{R}(n)$, uncorrelated with $\mathbf{w}(n)$. The algorithm is based on two recursive phases, which are briefly described below.

Prediction phase. Time update, providing *a priori* estimates for the next time step. The *a priori* state estimate $\hat{\mathbf{x}}(n+1|n)$ is calculated as:

$$\hat{\mathbf{x}}(n+1|n) = \mathbf{A}(n)\hat{\mathbf{x}}(n|n) + \mathbf{B}(n)\mathbf{u}(n), \tag{3}$$

and the *a priori* estimate of the state noise covariance $\mathbf{P}(n+1|n)$ is calculated as:

$$\mathbf{P}(n+1|n) = \mathbf{A}(n)\mathbf{P}(n|n)\mathbf{A}^T(n) + \mathbf{Q}(n). \tag{4}$$

The time update equations (3) and (4) project forward the state and covariance estimates from time step n to step $n+1$.

Correction phase. Measurement update, providing improved *a posteriori* estimates by incorporating a new measurement. Here n corresponds to what was $n+1$ in the prediction phase. The optimal Kalman gain $\mathbf{K}(n)$ is firstly calculated as:

$$\mathbf{K}(n) = \mathbf{P}(n|n-1)\mathbf{H}^T(n)\big[\mathbf{H}(n)\mathbf{P}(n|n-1)\mathbf{H}^T(n) + \mathbf{R}(n)\big]^{-1}; \tag{5}$$

then the *a posteriori* state estimate $\hat{\mathbf{x}}(n|n)$ is calculated as:

$$\hat{\mathbf{x}}(n|n) = \hat{\mathbf{x}}(n|n-1) + \mathbf{K}(n)\big[\mathbf{z}(n) - \mathbf{H}(n)\hat{\mathbf{x}}(n|n-1)\big], \tag{6}$$

finally, the *a posteriori* estimate of the covariance matrix $\mathbf{P}(n|n)$ is calculated as:

$$\mathbf{P}(n|n) = \big[\mathbf{I} - \mathbf{K}(n)\mathbf{H}(n)\big]\mathbf{P}(n|n-1), \tag{7}$$

where $\mathbf{I}$ corresponds to the identity matrix. When $n = 1$, the initial *a posteriori* estimate covariance $\mathbf{P}(1|1)$ is set to a determined constant value that represents a probable error magnitude of the initial estimation. A schematic representation of the Kalman filter algorithm is depicted in Figure 4.

2.2.2. Specific implementation within our block matching framework

Our KBM framework involves the integration of a Kalman filtering scheme within the speckle tracking method, in the objective to cope with the issue of speckle pattern decorrelation over time, and to avoid tracking errors due to progressive divergence. Our approach consists in estimating the optimal update of the gray-levels of the reference block pattern $\mathcal{B}_{ref}(n)$ in each frame of the sequence, prior to the block matching operation. The rationale of the proposed method is to exploit the cyclic 2D motion of the wall. Indeed, the moving tissues are expected to undergo a small deformation during the cardiac cycle, which modifies the corresponding speckle pattern, and to periodically recover their original appearance as they return to their

initial position. Therefore, our specific update strategy involves the combination of *i)* a fading memory scheme that takes into account the small deformation of the moving tissues during the cardiac cycle, and *ii)* a control signal that keeps track of the initial pattern of the block.

Each pixel of the block is considered separately, *i.e.* its state is estimated by an individual Kalman filter. Indeed, our aim is to avoid the influence between different regions of the block that may not undergo an identical gray level variation. Without loss of generality, we describe here the Kalman filtering scheme applied to a single (i-th) pixel of the reference block. In this situation, the vectors $\mathbf{x}$, $\mathbf{z}$, $\hat{\mathbf{x}}$, $\mathbf{u}$, $\mathbf{v}$ and $\mathbf{w}$, as well as the matrices $\mathbf{A}$, $\mathbf{B}$, $\mathbf{H}$, $\mathbf{P}$, $\mathbf{Q}$ and $\mathbf{R}$, are reduced to the dimension 1×1, *i.e.* scalars. Nevertheless, we keep the vectorial notations. A graphical representation of our specific Kalman filtering implementation is depicted in Figure 5.

The system state $\mathbf{x}(n)$ describes here the gray-level of the same i-th pixel at time n, representing an unknown noise-free value to be estimated. The observation $\mathbf{z}(n)$ corresponds to the measured noisy gray-level of the pixel at the location resulting from the previous block matching operation. The estimate $\hat{\mathbf{x}}(n)$ represents the gray-level of the i-th pixel used to construct the reference block.

According to our rationale, the control signal $\mathbf{u}$ is defined constant and equal to the initial gray-level reference $\hat{\mathbf{x}}(1)$ of the i-th pixel in $\mathcal{B}_{ref}(1)$. The state transition matrix $\mathbf{A}$ and the control matrix $\mathbf{B}$, reduced to scalars, are defined by positive constants α and β, respectively, such that $\alpha+\beta = 1$. The observation matrix $\mathbf{H}$ is also defined constant, the corresponding scalar being equal to 1. The observation noise $\mathbf{v}$ is assumed to correspond to the temporal variations of the gray-level, under the hypothesis that the tracked speckle pattern should ideally remain constant during the sequence. In our case, the covariance matrix $\mathbf{R}$ is reduced to a scalar σ_v^2, calculated at time step n as the variance of the $(n-1)$ previously estimated values of $\hat{\mathbf{x}}(n-1)$, multiplied by a positive constant scalar γ. When $n = 1$, $\sigma_v^2(1)$ is set to an initial empirically determined constant value that represents a probable noise magnitude. Similarly, the covariance matrix $\mathbf{P}$ is reduced to a scalar σ_x^2 and its initial value has been empirically determined. The process noise $\mathbf{w}$ represents the uncertainty of the process model and is also assumed to represent a slight variation of the gray-level. The covariance matrix $\mathbf{Q}$ is reduced to a constant scalar σ_w^2, the value of which reflects the magnitude of the expected gray-level variations. This value has also been empirically determined.

Our specific Kalman-based filter is integrated to our KBM algorithm using the above-detailed parameter settings. At each time step, the reference block $\mathcal{B}_{ref}(n)$ is thus updated, and then used to seek the position of the best matched block $\mathcal{B}(n+1)$ within the next image, as depicted in Figure 5. The 2D displacement $\hat{\mathbf{d}}(n+1)$ between

$\mathcal{I}(n)$ and $\mathcal{I}(n+1)$ is estimated by the block matching framework. To estimate sub-pixel displacements, the reference block and search window are interpolated by a factor 10 during the block matching operation.

2.3. Motion amplitude estimation

Once the 2D trajectory determined, relevant parameters need to be deduced. Previous work suggests that the longitudinal motion amplitude actually is a relevant parameter, *i.e.* it corresponds to a clinical information about vascular health. In our study both longitudinal and radial motion amplitude parameters have been measured from the corresponding trajectory for each subject. The respective amplitudes ΔX and ΔY were calculated as the average value of the peak-to-peak amplitudes measured in two cardiac cycles, for both longitudinal and radial directions (Fig. 6). Such an evaluation of dynamical parameters derived from the trajectory is expected to characterize the potential of our method to provide clinically useful markers.

2.4. Acquisition of in vivo image data

2.4.1. Study population

Fifty-seven healthy volunteers, as well as 25 patients at high cardiovascular risk and likely to develop atherosclerosis, were involved in this study. The healthy volunteers were 24 males and 33 females, aged from 19 to 63 years (mean age 37.9 $\pm$ 14.1 years). The at-risk patients were 16 males and 9 females aged from 34 to 73 years (mean age 56.2 $\pm$ 10.5 years). The inclusion criterion for the at-risk patients was the presence of one of the following diseases diagnosed at least 1 year before (Ford, 2005): the metabolic syndrome, or type 1 or 2 diabetes. No other criterion, including clinical characteristics, was used to select these subjects. The healthy volunteers were cardiovascular risk factor-free (tobacco use, hypercholesterolemia, diabetes, hypertension or particular family history) as assessed by an oral questionnaire. Informed consent was obtained from all participants. The study was conducted in compliance with the requirements of our institutional review board and the ethics committee.

2.4.2. Acquisition of carotid artery ultrasound sequences

Ultrasound acquisition was performed with a medical scanner (Antares, Siemens, Erlangen, Germany), equipped with a 7.5- to 10-MHz linear array transducer. Longitudinal B-mode image sequences of the left CCA were acquired for all subjects. After a 15 minutes rest, the subjects were examined in the supine position with the neck extended and rotated 45° to the contralateral side. The transducer was centered on the CCA, in the longitudinal plane, 2 cm distant from the carotid bulb. The absence of atheromatous plaques in the imaged area was assessed by a medical

doctor. Images were recorded through at least two consecutive full cardiac cycles. To avoid the influence of the movement due to breathing, the subjects performed a breath hold during the acquisition. The following instrumentation settings were maintained for all acquisitions: the dynamic range was 65 dB, the sequence frame rate was 26 fps, the pixel size in both radial and longitudinal directions was 30 μm. The sequences were stored digitally and transferred to a commercial computer for off-line image analysis. No subject was rejected *a priori* from the study.

2.5. Evaluation of the accuracy of our method

For each sequence, reference trajectories were generated in the objective to evaluate the accuracy of our KBM method, despite the lack of ground truth inherent to clinical imaging. Each reference trajectory corresponded to the averaged trajectories resulting from the manual tracings performed by three experienced observers. The inter- and intra-observer variability of these manual tracings was also assessed, one expert performing twice the manual tracking operation for each sequence. Moreover, the results of our KBM method were also compared to those obtained with six other state-of-the-art techniques. All resulting 2D trajectories were stored for further analysis.

2.5.1. Trajectory reference

In the objective to quantify the tracking accuracy of our KBM method, a reference 2D trajectory was constructed over the full length of each sequence. First, a point $\mathbf{p}(1)$ to be tracked, located in the intima-media complex of the carotid distal wall, was selected by the observer O_1 in the first frame of each sequence (Fig. 3). The observer was asked to select a well distinguishable speckle pattern remaining visually perceptible during the whole sequence, in order to make sure that each observer will be able to identify the same target all along the sequence. Then, this initial point was tracked over the full length of the sequence, both by the automated KBM processing and by the three observers O_1, O_2 and O_3, blinded to the automatic results. For each sequence, the 2D trajectory reference was finally constructed by averaging the results from the three observers, in both radial and longitudinal directions. All resulting 2D trajectories were stored for further analysis. The reference motion amplitude of each sequence was also defined as the peak-to-peak amplitude of the corresponding reference trajectory (Fig. 6). Although we focus in this work on the longitudinal motion amplitude, which corresponds to a risk marker, we also evaluate the radial amplitude. The latter does not represent a clinical information when only estimated on a single wall. Nevertheless, its accuracy also gives an insight to the overall accuracy of the estimated trajectories.

2.5.2. Comparison with other methods

We compared our KBM method with six state-of-the-art tracking methods. We do not pretend to have exactly re-implemented all these methods, which is often not feasible due to the lack of full details in the publications. Instead, we aimed at evaluating the influence of various parameters and concepts. To perform a fair comparison, all the methods considering a single block were initialized with a block centered in the same previously described initial point $\mathbf{p}(1)$, and the methods considering multiple blocks were applied on a region of the wall that included $\mathbf{p}(1)$.

Block matching without Kalman estimator. A classical BM algorithm (that is to say without Kalman-based update of the reference block) was applied to track the same initial point as our KBM method. To assess the influence of the block and search-window size, three different configuration settings, hereafter denoted as BM, BM_{bis} and BM_{ter}, were used. These respectively correspond to the parameters settings used in *i)* the KBM framework proposed in the present work, *ii)* the echo tracking method proposed in (Cinthio et al., 2005), and *iii)* the block matching method proposed in (Golemati et al., 2003).

Kalman filtering without control signal. Let us recall that the main feature of our KBM method is the use of a hard memory of the system *via* the control signal $\mathbf{u}$ (Eq. 1), which was not used in the update scheme of the seminal work by Gastounioti et al. (2011). In order to assess the influence of this signal, we switched it off in our implementation by setting the control matrix to zero ($\beta = 0$). This version, hereafter denoted as KBM_{bis}, was also applied to track the same initial point of each sequence.

Multi-block matching. All the previously mentioned BM and KBM methods can be classified within the Lagrangian approach, as they all attempt to follow a single target along its trajectory across the spatio-temporal domain. They are all confronted with the problem of speckle decorrelation, which requires a careful design of the update scheme for the reference block. As summarized in Section 1.2.3, the MBM framework (Zahnd et al., 2012) attempts to cope with this problem *via* an Eulerian approach, *i.e.* by estimating the motion at fixed locations within the spatial domain. It involves a contour segmentation scheme aiming to extract the contours of the intima-media complex. At each time step, 16 regularly spaced blocks are repositioned within the intima-media complex, with the upper edge adjacent to the lumen-intima contour. The displacement of each block is estimated independently by seeking the most similar block in the next image, and the resulting displacement of the wall is finally calculated as the median value of all the 16 estimates. In this approach, no memory is used in the update scheme, *i.e.* $\mathcal{B}_{ref}(n) = \mathcal{B}(n)$.

Velocity Vector Imaging. The VVI commercial software was originally designed to assess the heart dynamics in US B-mode image sequences. Although it has not been optimized to assess the arterial wall motion, it was recently used to investigate the CCA motion (Svedlund et al., 2011; Svedlund and Gan, 2011). We therefore also compared it with our method, using a similar operating mode. The virtual transducer used by the software was centered on the top of the screen (Fig. 7a). The horseshoe-shaped line, originally designed to represent the boundary of the heart (Fig. 7b), was positioned on the proximal and distal walls with a total of 20 control points. One of its segments was centered on the initial position of the point $\mathbf{p}(1)$ previously specified by the observer O_1 (Fig. 7a). The 2D motion of the distal intima-media complex was automatically estimated within the full length of this segment roughly corresponding to 5 mm. The VVI software displays but does not export the resulting trajectory (Fig. 7c), so this information was not available for our study. Only the trajectory amplitudes in the longitudinal (ΔX) and radial (ΔY) directions, automatically calculated by the VVI software, were stored for further analysis. We limited this analysis to the healthy volunteers subset, as the results were relatively poor and the VVI method is relatively labor-consuming and not fully reproducible, due to the manual placement of the control points. The reproducibility was assessed by re-running the computation after a new choice of the control points.

2.6. Parameter settings

Each method was applied on all the sequences with unchanged parameter settings. These settings are specified below.

Block matching. The block, search window, and margin dimensions that were used for our KBM framework as well as the other methods (*i.e.* KBM_{bis}, MBM, BM, BM_{bis}, and BM_{ter}) are detailed in Table 1. For all methods, the block and window were systematically interpolated by a factor 10, and the similarity criterion was the normalized sum of squared differences (NSSD).

Kalman filter. Our KBM method used the following settings: state-transition matrix coefficient $\alpha = 0.85$; control matrix coefficient $\beta = 0.15$; initial observation-noise variance $\sigma_v^2(1) = 25$ (*i.e.* corresponding to a standard deviation of 5 for the gray level, whose range in the image is [0, 255]); process-noise variance $\sigma_w^2 = 25$; initial estimate variance $\sigma_x^2(1|1) = 25$; covariance matrix coefficient $\gamma = 2$. The KBM_{bis} method used the same settings except for $\alpha = 1$ and $\beta = 0$.

2.7. Statistical analysis

The Mann-Whitney U test was used to compare the values of the longitudinal displacement amplitude ΔX, between healthy volunteers and at-risk patients. The

value $p < 0.05$ was considered to indicate a statistically significant difference. All statistical analyses were performed using Intercooled Stata 10.0 (StataCorp LP, College Station, TX, USA).

3. Results

As previously described, the point $\mathbf{p}$ selected by the observer O_1 within the intima-media complex in the first frame of each sequence, was tracked by the three observers O_1, O_2 and O_3, as well as by our KBM method and six other methods (*i.e.* KBM$_{bis}$, MBM, BM, BM$_{bis}$, BM$_{ter}$, and VVI). One sequence, from the healthy group, was excluded *a posteriori* from the evaluation, as the longitudinal trajectories resulting from the observers' tracings were so much different from each other that a reliable reference could not be established. In the remaining 81 sequences, the accuracy of the methods was evaluated in two ways: by a point-wise comparison of the trajectories and by a global comparison of the resulting amplitudes. The tracking error was defined as the absolute difference between the estimated coordinates of the tracked point and the reference, in each frame of the sequence, for both radial and longitudinal directions. For each trajectory, including the reference, the longitudinal and radial motion amplitudes were calculated by averaging the peak-to-peak amplitudes from two different cardiac cycles (Fig. 6). The amplitude estimation error was defined as the difference between the estimated and reference amplitudes, for both radial and longitudinal directions.

Before the detailed presentation of the quantitative results, let us show some qualitative examples. The trajectories estimated with our method demonstrated a good similarity with the reference, as depicted in Figure 8. This figure also displays the trajectories resulting from the other methods applied onto the same sequences. To limit the number of curves, instead of the three observers' trajectories, only the reference trajectory and the standard deviation (error bars) introduced by the observers are displayed. In each case, the reference trajectories present a more or less visible "drift", *i.e.* they do not systematically return to their initial position at the end of each cardiac cycle, probably due to a slight contraction of the subject's neck muscles. Nevertheless, the KBM method kept accurate track of the targeted point. In comparison, the other methods generated rather large tracking errors, visible as an increasing divergence (KBM$_{bis}$, BM), a high jitter (BM$_{bis}$), or a reduced motion amplitude (MBM, BM$_{ter}$).

As for the processing time, it is proportional to the number of frames in the sequence. The average number of frames in the considered 81 sequences was 116 ± 34 (range $66 - 194$). Implemented in Matlab (MATLAB 7.13, The MathWorks Inc., Natick, MA, 2011), our KBM method required, on average, 66 seconds to process the whole sequence, including the interactive initialization, while the manual tracking by the experts took 161 seconds, on average.

3.1. Trajectory estimation

Figure 9 shows a good correlation between the estimated trajectories and the reference. However, while the estimation of the radial motion component was always successful ($R = 0.993$), the estimation of the longitudinal component performed rather poorly for two sequences from the healthy volunteers group, which explains a weaker correlation ($R = 0.956$). The mean absolute tracking errors, in both longitudinal and radial directions, for our KBM method and the other methods (*i.e.* KBM$_{bis}$, MBM, BM, BM$_{bis}$ and BM$_{ter}$), are displayed in Table 2. The errors of our method were of the same order of magnitude as the inter- and intra-observer variability, whereas the errors generated by the other methods were systematically and noticeably greater.

It is useful to compare the tracking errors with the peak-to-peak amplitude of the trajectories. The mean values (± standard deviation) of the reference longitudinal and radial motion amplitudes in all the 81 assessed subjects were $\overline{\Delta X}_{REF} =$ 634 (±302) μm and $\overline{\Delta Y}_{REF} = 373$ (±179) μm, for the longitudinal and radial directions, respectively. More specifically, the reference longitudinal and radial motion amplitudes were 716 (±275) μm and 388 (±198) μm for the 56 healthy volunteers, and 450 (±283) μm and 339 (±122) μm for the 25 at-risk patients, respectively. Putting together the ratios between the absolute tracking errors at each time point of each individual sequence and the longitudinal and radial amplitude of the corresponding individual reference trajectories, the mean values (± standard deviation) were: 15(±20)% of ΔX_{REF} and 7(±9)% of ΔY_{REF} for the 56 healthy volunteers; 20(±20)% of ΔX_{REF} and 7(±9)% of ΔY_{REF} for the 25 at-risk patients; and 16(±20)% of ΔX_{REF} and 7(±9)% of ΔY_{REF} for all the 81 subjects, respectively.

3.2. Motion amplitude

Table 3 summarizes the errors of the motion amplitudes estimated by our KBM method, as well as by the other methods (*i.e.* KBM$_{bis}$, MBM, BM, BM$_{bis}$, BM$_{ter}$, and VVI), as compared to the reference. The errors of our method were of the same order of magnitude as the inter- and intra-observer variability, and very close to the corresponding errors in the position tracking reported in Table 2. Moreover, our method systematically showed a better accuracy in comparison with all the other compared methods. Putting together the ratios between the amplitude errors generated on each individual sequence and the amplitude of the corresponding individual reference trajectory, the mean values (± standard deviation) were: 12(±11)% of ΔX_{REF} and 6(±7)% of ΔY_{REF} for the 56 healthy volunteers; 14(±11)% of ΔX_{REF} and 6(±5)% of ΔY_{REF} for the 25 at-risk patients; and 13(±11)% of ΔX_{REF} and 6(±7)% of ΔY_{REF} for all the 81 subjects.

Figure 10 shows a good correlation between the estimated amplitudes and the reference. For the already mentioned reasons (loss of the longitudinal track in two sequences), the correlation was better in the radial direction (R=0.992) than in the longitudinal direction (R=0.952). The Bland and Altman plots (Fig. 11) demonstrate an overall good agreement of the amplitudes between our method and the reference, with the 95% confidence intervals of 189 μm (30% of $\overline{\Delta X}_{REF}$) and 46 μm (12% of $\overline{\Delta Y}_{REF}$) for the longitudinal and radial direction, respectively. Figure 11 also shows that, on average, the estimated amplitudes were slightly under-evaluated in comparison to the reference: $-31\,\mu$m and $-6\,\mu$m in the longitudinal and radial directions. This under-evaluation was not larger than the pixel size and small in comparison with the corresponding amplitudes: -5% of $\overline{\Delta X}_{REF}$ and -2% of $\overline{\Delta Y}_{REF}$, respectively.

The dispersion of the estimated motion amplitude, for our KBM method, the six other methods (*i.e.* KBM$_{bis}$, MBM, BM, BM$_{bis}$, BM$_{ter}$, and VVI), and the three observers, is displayed in Figure 12 (please remind that the VVI software was only applied on the sequences from the 56 healthy volunteers). The boxes and error bars representing the distribution of the errors w.r.t. the reference are tighter for the observers than for our KBM method, which is quite normal, as the reference was built up based on the observers' tracings. Nevertheless, the boxes and error bars for our KBM method remain relatively narrow and close to those for the observers, while the distribution of the errors resulting from the other methods shows a greater dispersion with a larger average under-evaluation of the longitudinal and radial directions amplitudes: $-106\,\mu$m and $-15\,\mu$m for KBM$_{bis}$; $-215\,\mu$m and $-29\,\mu$m for MBM; $-162\,\mu$m and $-41\,\mu$m for BM; $-60\,\mu$m and $-15\,\mu$m for BM$_{bis}$; $-335\,\mu$m and $-76\,\mu$m for BM$_{ter}$; $-244\,\mu$m and $-83\,\mu$m for VVI.

3.2.1. Statistical analysis

The result of the Mann-Whithney U test demonstrated that the peak-to-peak amplitude of the longitudinal motion ΔX, estimated with our KBM method, was significantly reduced in at-risk patients compared to healthy volunteers ($408 \pm 281\,\mu$m *vs* $643 \pm 274\,\mu$m, $p < 0.0001$, Fig. 13).

Let us note that the peak-to-peak amplitude of the radial motion ΔY does not correspond to the cross-sectional diameter change, as the motion of only one wall was assessed, therefore no statistical comparison of this parameter between the two groups was realized.

4. Discussion and Conclusion

4.1. On the proposed method

To estimate the 2D motion of the arterial tissues, we introduced a novel block matching method that involves a specific Kalman filtering scheme. The Kalman filter is used to optimally update the gray levels of the reference block containing the tracked pattern. This update strategy is performed pixel-wise, *i.e.* each pixel of the reference block is considered independently, in order to avoid the influence between different parts of the block that may not follow the same gray-level variation. By using the initial pattern appearance as control signal, we have successfully addressed the problem of speckle decorrelation inherent to US imaging of moving tissues: the reference block appearance evolves to take into account the observed variations, but this evolution does not lead to divergence.

Similarly to the previously published work, we have chosen to estimate one single trajectory that is expected to characterize the stiffness of the whole arterial wall section. To this purpose, we recommend to select a single salient echo, which enables the user to visually check the correctness of the tracking result and probably makes the tracking more robust. Although the at-risk patients are often less echogenic than the healthy subjects, such a well-distinguishable echo scatterer was perceptible through the entire sequence in all but one out of the 82 subjects involved in our evaluation. Nevertheless, despite its overall best performance, our method poorly estimated the longitudinal motion in two sequences from the healthy group. Therefore, we recommend to systematically perform a visual inspection, once the process is over, to check whether: *i*) the resulting 2D trajectory is cyclic and reproducible, and *ii*) the estimated block location is always superimposed onto the pattern of interest. These checking operations can be performed very easily and quickly thanks to a smart implementation, allowing the user to display the results.

As the use of a salient point was mandatory to perform reliable manual tracking and build the reference trajectories, we did not investigate the variability of the estimated wall motion when varying the initial point to be tracked. Moreover, our experience suggests that different sections of the wall actually undergo slightly different displacements. A thorough investigation of this phenomenon was beyond the scope of this article, as well as the assessment of the method's sensitivity to varying imaging parameters (*i.e.* gain, central frequency, frame rate, or pixel size).

In our study, the sequences were acquired with the same ultrasound scanner and by the same medical doctor. We expect that some parameters of the algorithm have to be adjusted if the image acquisition settings change. Namely, the Kalman model provides optimal results if the covariance matrices $\mathbf{P}$, $\mathbf{Q}$ and $\mathbf{R}$ (*cf* Section 2.2.2)

correctly reflect the noise levels of the system. The corresponding variances σ_x^2, σ_w^2 and σ_v^2 have been empirically determined (*cf* Section 2.6), based on sequences acquired in the same conditions (*cf* Section 2.4.2), and are likely not to be optimal if the actual gain and noise levels change significantly. Similarly, the block $\mathcal{B}$ has to encompass the tracked salient echo scatterer (Fig. 3). Its size was set empirically in our study and may require modifications depending on the spatial definition of the actual ultrasound scanner. One limitation of our method is related to the assumption that the tracked pattern periodically recovers its initial appearance and location. This assumption holds if the ultrasonographer is experienced enough to hold the probe immobile with respect to the carotid artery.

4.2. On the compared methods

The previously published work mainly differs from our method in two aspects: block/window size and update strategy.

Concerning the update strategy, we compared four approaches, using the same block size. Three of them, namely KBM, KBM$_{bis}$ and BM, perform a Lagrangian tracking of a single block, whereas the fourth one, MBM (Zahnd et al., 2012), rather falls into the Eulerian motion-estimation category and uses multiple blocks. Our KBM method performed the best, while KBM$_{bis}$ was ranked second, due to a progressive divergence in the trajectory estimation (Fig. 8). As the latter method uses a Kalman filtering scheme without control signal $\mathbf{u}$, similarly to (Gastounioti et al., 2011), this result illustrates how important it is to integrate the initial pattern $\mathcal{B}_{ref}(1)$ in the update strategy of the reference block. The classical BM method, without Kalman filter, generated larger errors and showed an increased divergence (Fig. 8), caused by cumulating the successive errors due to the "hard" update (*i.e.* using the block found in the previous frame as reference). Despite the use of the same "hard" update, MBM performed almost as well as KBM$_{bis}$ from the tracking accuracy point of view. This is probably a beneficial combination of two effects: *i*) longitudinal block repositioning at fixed grid locations, according to the Eulerian approach, which partly avoids cumulating the successive errors, and *ii*) the use of multiple blocks, which partly compensates the incorrect estimates. However, the counterpart of combining the estimates from multiple blocks is that large displacements are discarded and the motion amplitude is thus significantly underestimated.

As for the block size, in our KBM method we have chosen to adapt its width (1.50 mm) to the typical width of salient echo scatterers and its height (0.30 mm) to the thickness of the intima-media complex (the latter in the objective to avoid the inclusion of neighboring differently moving tissues). The same size was used by the BM method and compared to the variants using the same update strategy

with a smaller or larger block size: BM_{bis} and BM_{ter}, respectively. The largest tracking errors were obtained with reduced block and window dimensions (BM_{bis}), as proposed in (Cinthio et al., 2005). Several mismatches can be observed as a jitter in the trajectory (Fig. 8). Cinthio et al. (2005) have previously reported very accurate results, but the images were acquired on a different scanner, with a very careful protocol, which resulted in a better quality. We therefore suggest that such a small block size leads to a high noise-sensitivity and is not well suited to current clinically acquired sequences. Conversely, a large block/window size (BM_{ter}), such as the one used by Golemati et al. (2003), is more robust to noise, but the estimated trajectory does not achieve the entire motion amplitude. Additional errors are due to the fact that the block encompasses several differently moving regions.

It is interesting to remark that comparable tracking errors (*e.g.* KBM_{bis} *vs* MBM or BM *vs* BM_{ter}) do not necessarily imply similar amplitude errors, and *vice-versa*. We have observed that a method that diverges (*i.e.* progressively tracks a pattern different than the initial one), may nevertheless reasonably well capture the motion amplitude (Fig. 8). This mainly happens for the methods that use a reduced spatio-temporal support, such as KBM_{bis} and BM. Conversely, a method that provides stable trajectories, thus generating relatively small tracking errors, may fail to capture the full dynamics of the motion. Such under-evaluation of the motion amplitude rather occurs with methods using a larger spatial support, such as MBM and BM_{ter}.

We also included in our evaluation the VVI method that was recently used to study the longitudinal motion of the arterial wall in carotids (Svedlund and Gan, 2011; Svedlund et al., 2011), although its principle can hardly be compared with block-matching methods. However, it ranked penultimate, which can be explained by the fact that the VVI commercial software was not optimized for this application and also by the use of a relatively large spatial support.

As expected, both motion tracking and amplitude estimation errors generated by all methods, including KBM, were greater in the longitudinal direction compared to the radial direction. This is caused by the previously mentioned two factors that contribute to make challenging the assessment of the longitudinal arterial-wall motion in *in vivo* US images: *i*) lack of acoustic interfaces in this direction, and *ii*) shape of the US-scanner PSF.

4.3. On the clinical applications

As the longitudinal motion has been evidenced recently (Persson et al., 2003), relatively few (semi)automatic methods have been proposed to investigate clinically this phenomenon. Nevertheless, although they were less accurate and/or more noise-sensitive than our method, the published studies have demonstrated that the longitu-

dinal motion amplitude can provide relevant and complementary information about arterial physiopathology. In particular, according to Svedlund et al. (2011) the longitudinal motion amplitude can predict 1-year cardiovascular outcome independently of other risk factors. It has also been shown that this parameter undergoes profound changes in response to catecholamines (Ahlgren et al., 2009, 2012). The authors have deduced from this finding that the mental stress, which is considered as a risk factor for the cardiovascular disease, is correlated with the endothelial shear strain (calculated using the longitudinal motion amplitudes at the inner and outer boundaries of the intima-media complex). Based on three clinical studies, our team has shown that the amplitude of the longitudinal motion does not simply replicate the information provided by traditional risk markers, but is rather likely to represent a complementary marker of early arterial wall abnormalities. In the first study (Zahnd et al., 2011a), young healthy volunteers were compared to elderly diabetic patients. This proof of concept confirmed that the longitudinal motion amplitude was significantly reduced in at-risk patients compared to healthy controls. In the second study (Zahnd et al., 2011b), three populations were compared: young healthy subjects, elderly healthy subjects and elderly diabetic patients, using the shear index (a parameter based on the longitudinal motion amplitudes) and the distensibility (conventional marker based on the radial motion). When using the former, a significant difference has been found between both healthy populations and the diabetic patients, but not between young and elderly healthy volunteers. When using the latter, a significant difference has been found between the young healthy volunteers and both elderly populations, but not between the diabetic patients and the elderly healthy volunteers. In the third study (Zahnd et al., 2012), patients with periodontal disease were compared to a control group of the same age, using the shear index and the distensibility. The former evidenced a significant difference between the patients and the control group, while no significant difference was found when using the latter parameter.

The goal of this article was to present our KBM method and to evaluate its accuracy, but neither to tackle a specific new clinical problem, nor to assess the relevance of the longitudinal motion as compared to traditional cardiovascular risk markers. Patients at high cardiovascular risk were included in the study because they are often less echogenic, which leads to a decreased image quality. A "side effect" was to confirm that the longitudinal motion amplitude, estimated using this method, was significantly reduced in at-risk patients compared to healthy volunteers. Now that the KBM method has demonstrated its accuracy, it can be used to investigate the arterial wall motion more thoroughly. In particular, beyond the motion amplitude, it can be interesting to explore parameters characterizing the shape of the trajectories.

More generally, the cause of wall longitudinal motion still remains to be confirmed. We suggest that blood friction, creating a tangential force at the surface of the wall, only constitutes a minor contribution. Indeed, we propose that the antegrade wall longitudinal motion may rather be coupled to the radial systolic stretching caused by the blood volume influx (this phenomenon being different to the propagation of the pulse wave, generated by the systolic stroke volume). We also suggest that the retrograde wall longitudinal motion is induced by a first protosystolic backward motion caused by the apical motion of the aortic valve annulus, and a second mesosystolic backward motion caused by the reflected wave. Future applications of our KBM method may contribute to a better understanding of this phenomenon.

4.4. Conclusion

The longitudinal motion of the arterial wall, which remains a challenging parameter to assess with accuracy, is likely to constitute a novel complementary and relevant clinical information about vascular health. To address this problematic and investigate this phenomenon, we have presented a method to assess *in vivo* the 2D motion of the arterial wall, and evaluated it on the distal wall of 82 US B-mode sequences of human CCA. Our method involves a Kalman-based block matching framework, requires minimal user interaction, and provides results of the same order of accuracy as those manually obtained by experienced observers, while remaining much faster and fully reproducible. The proposed method can already constitute a reliable technique to investigate vascular health in clinical studies.

Figures

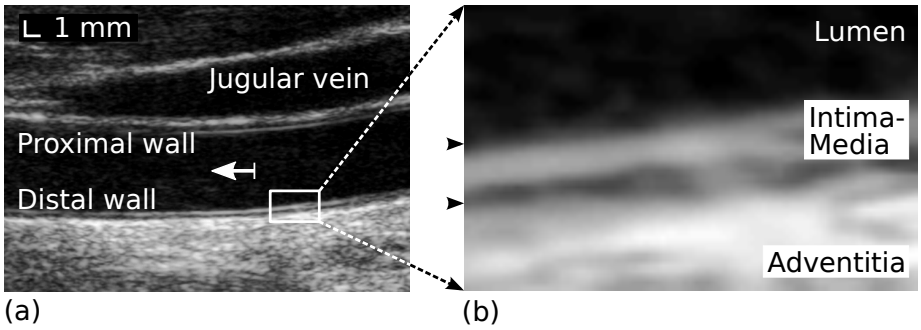

Figure 1: Structure of the CCA. (a) Ultrasound B-mode image of a longitudinal section. The blood direction is indicated by the white arrow. (b) Detailed region of the distal wall, showing the lumen and the three tissue layers. The location of the lumen-intima and the media-adventitia interfaces is displayed by the two black triangles.

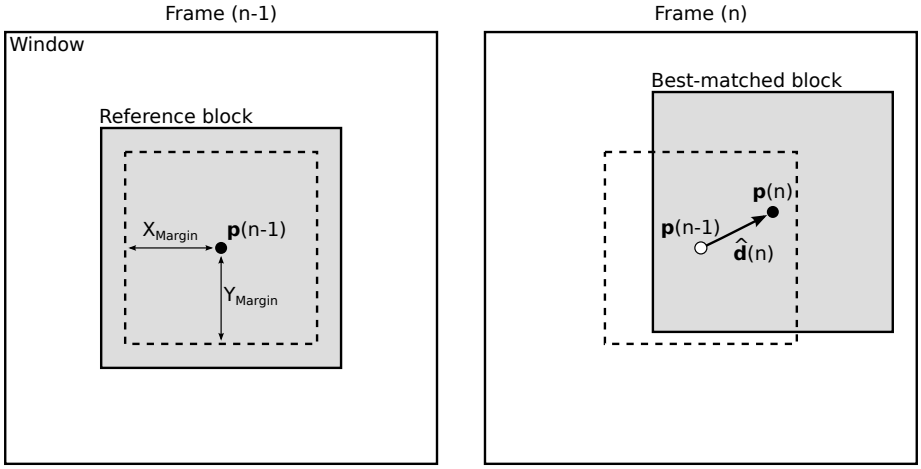

Figure 2: Block matching schematic diagram. The displacement $\hat{\mathbf{d}}(n)$ corresponds to the motion from the reference block centered on the point $\mathbf{p}(n-1)$ to the location of the best matched block centered on the point $\mathbf{p}(n)$ between the $(n-1)^{\text{st}}$ and the n^{th} frames. The search window corresponds to the whole investigated neighborhood defined by the maximal displacement margins $[X_{\text{Margin}}, Y_{\text{Margin}}]$, delimited by the dashed square.

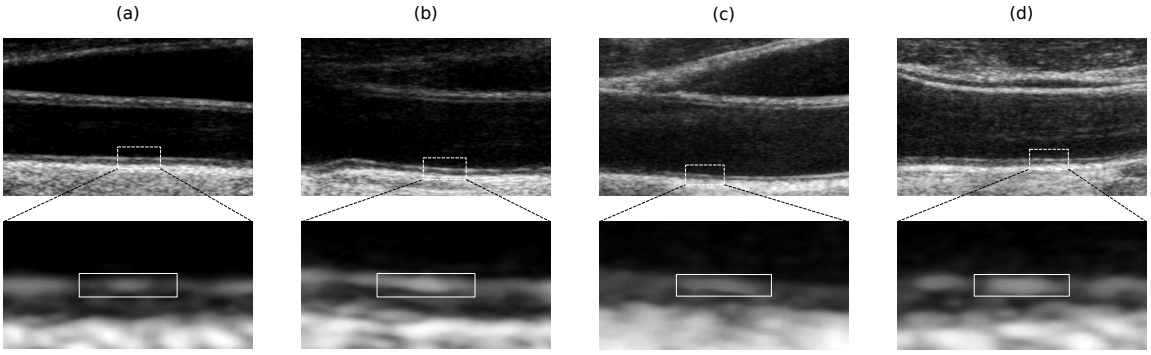

Figure 3: Example of US B-mode images of the CCA, from two healthy volunteers (a, b) and two at-risk patients (c, d). For each subject, the enlarged region (bottom) corresponds to the white dashed rectangle (top). Within the intima-media complex of the distal wall, the block $\mathcal{B}$ (white solid rectangle, $1.50 \times 0.30\,\mathrm{mm}^2$) is centered on the tracked point $\mathbf{p}$, *i.e.* an echo scatterer generating a well-distinguishable speckle pattern.

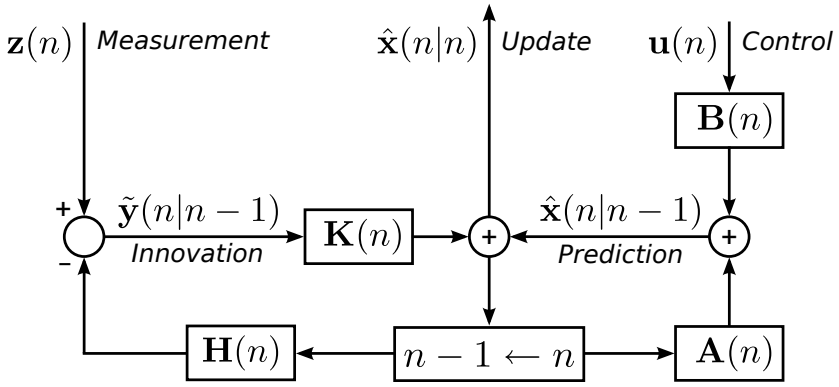

Figure 4: Schematic representation of the Kalman filter algorithm. In our context, the measurement $\mathbf{z}(n)$ corresponds to the current best-matched block $\mathcal{B}(n)$, the control signal $\mathbf{u}(n)$ corresponds to the initial reference block $\mathcal{B}_{ref}(1)$, and the update $\hat{\mathbf{x}}(n|n)$ corresponds to the reference block $\mathcal{B}_{ref}(n)$.

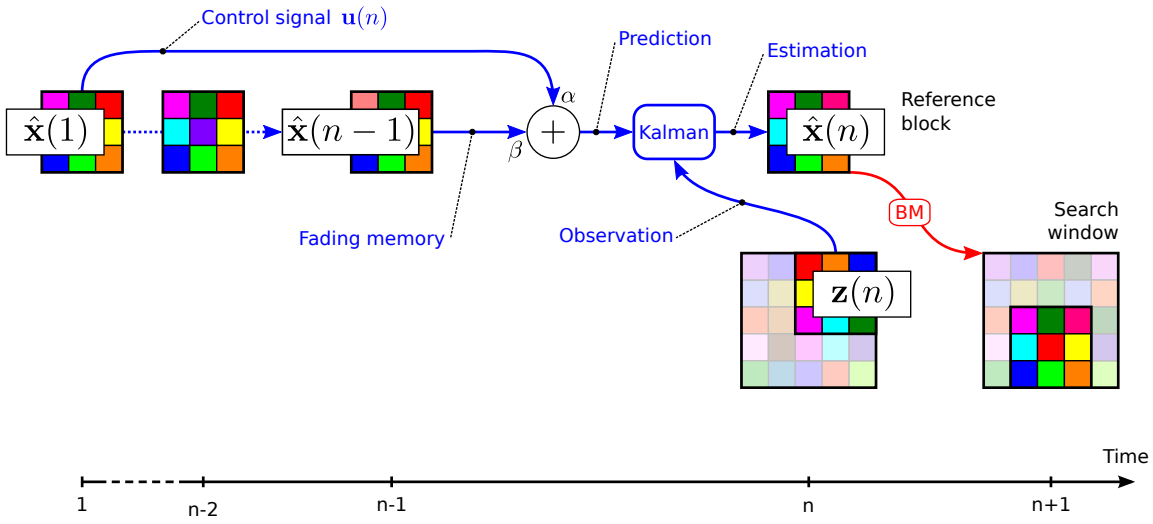

Figure 5: Illustration of our specific Kalman Block Matching (KBM) method. The Kalman filter is used pixel-wise to estimate the gray level $\hat{\mathbf{x}}(n)$ of the reference block $\mathcal{B}_{ref}(n)$, given the previous estimation $\hat{\mathbf{x}}(n-1)$, the control signal $\mathbf{u}(n)$ (i.e. the initial reference block $\mathcal{B}_{ref}(1)$), and the observation $\mathbf{z}(n)$ (*i.e.* the best-matched block $\mathcal{B}(n)$). A block matching (BM) operation is finally carried out to estimate the displacement between the two considered subsequent frames, using the estimated reference block.

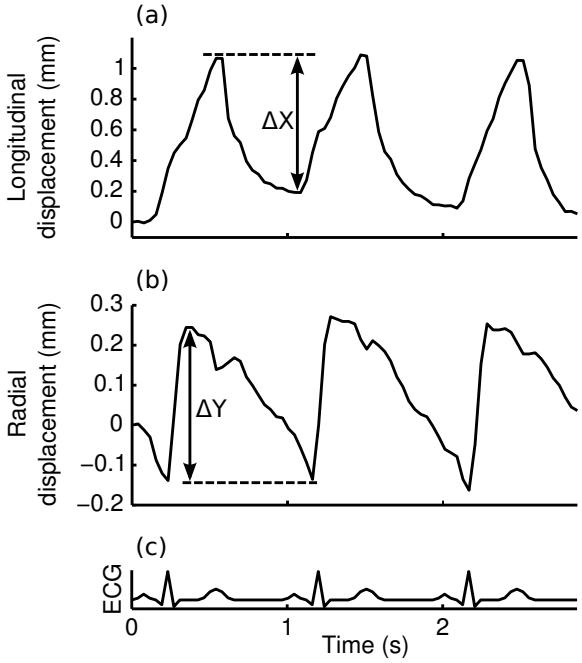

Figure 6: Example of trajectories and respective amplitudes: ΔX, in the longitudinal direction (a), and ΔY in the radial direction (b), with the corresponding ECG (c).

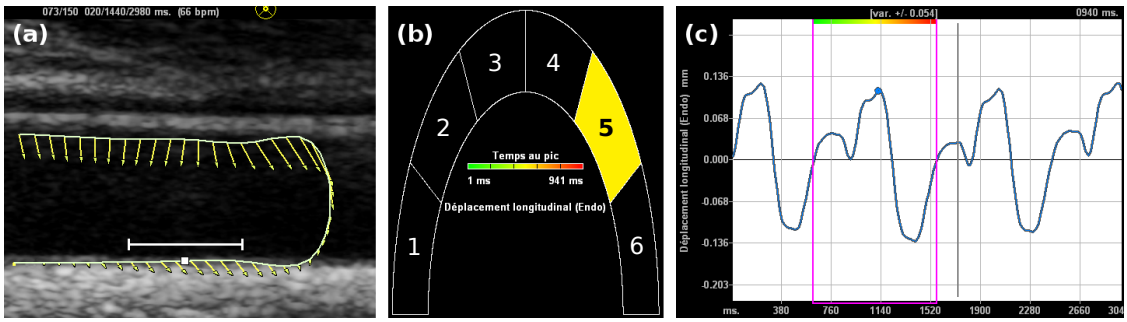

Figure 7: Velocity Vector Imaging (VVI) commercial software. (a) Longitudinal view of the carotid artery, with the position of the tracked point $\mathbf{p}$ previously selected by the observer O_1 (white square). The horseshoe-shaped set of control points is positioned in order to center the tracked point $\mathbf{p}$ in the middle of the segment identified by a white bar and corresponding to the fifth zone (yellow) in (b). (b) Representation of the six zones defining the horseshoe-shape, where the 5^{th} one (yellow) corresponds to the white bar in (a). (c) Resulting longitudinal trajectory of the region corresponding to the 5^{th} segment.

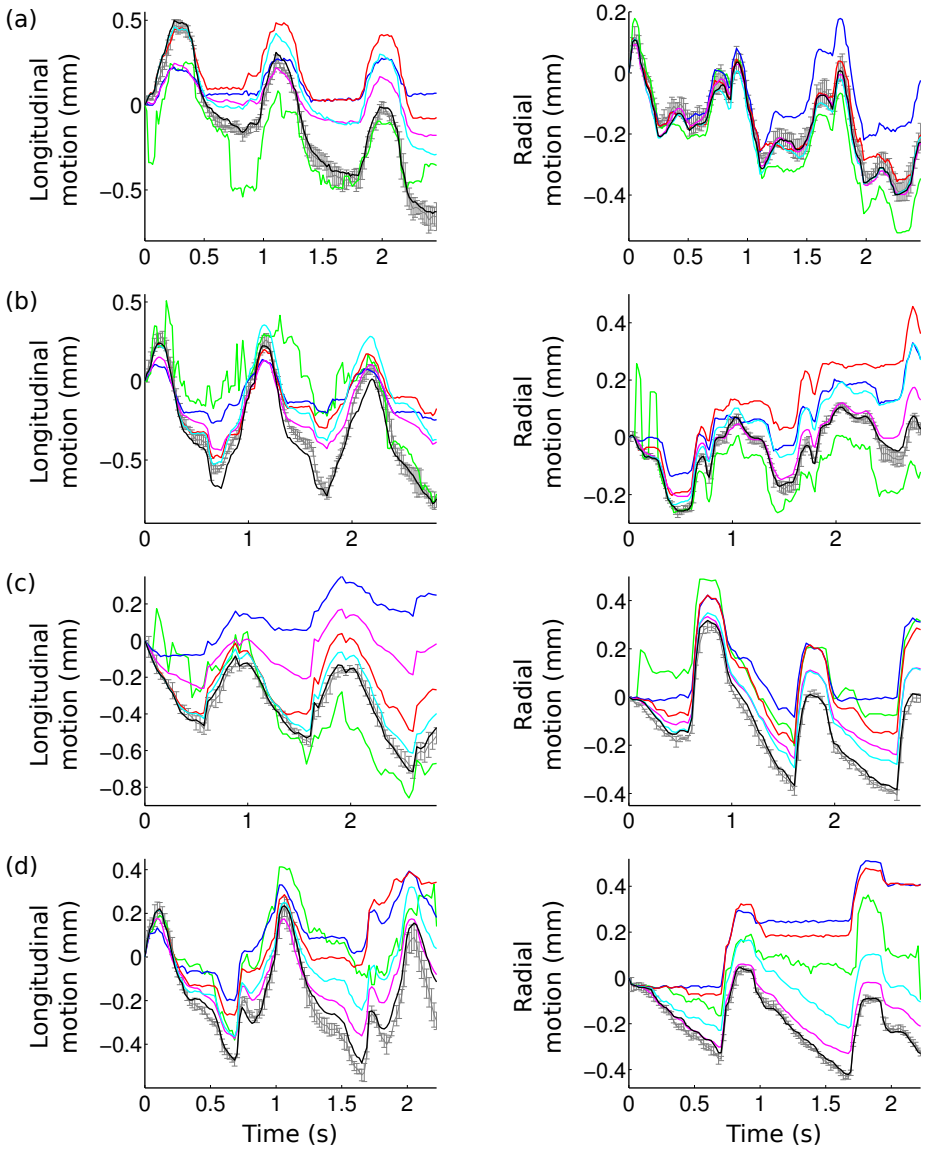

Figure 8: Results of the trajectory estimation over several cardiac cycles, from two healthy volunteers (a, b) and two at-risk patients (c, d), in the longitudinal (left) and radial (right) directions, for our KBM method (black), as well as for KBM$_{bis}$ (cyan), MBM (magenta), BM (red), BM$_{bis}$ (green), and BM$_{ter}$ (blue). The reference trajectory (gray) is displayed together error bars representing the variability (standard deviation) introduced by the three observers O_1, O_2 and O_3.

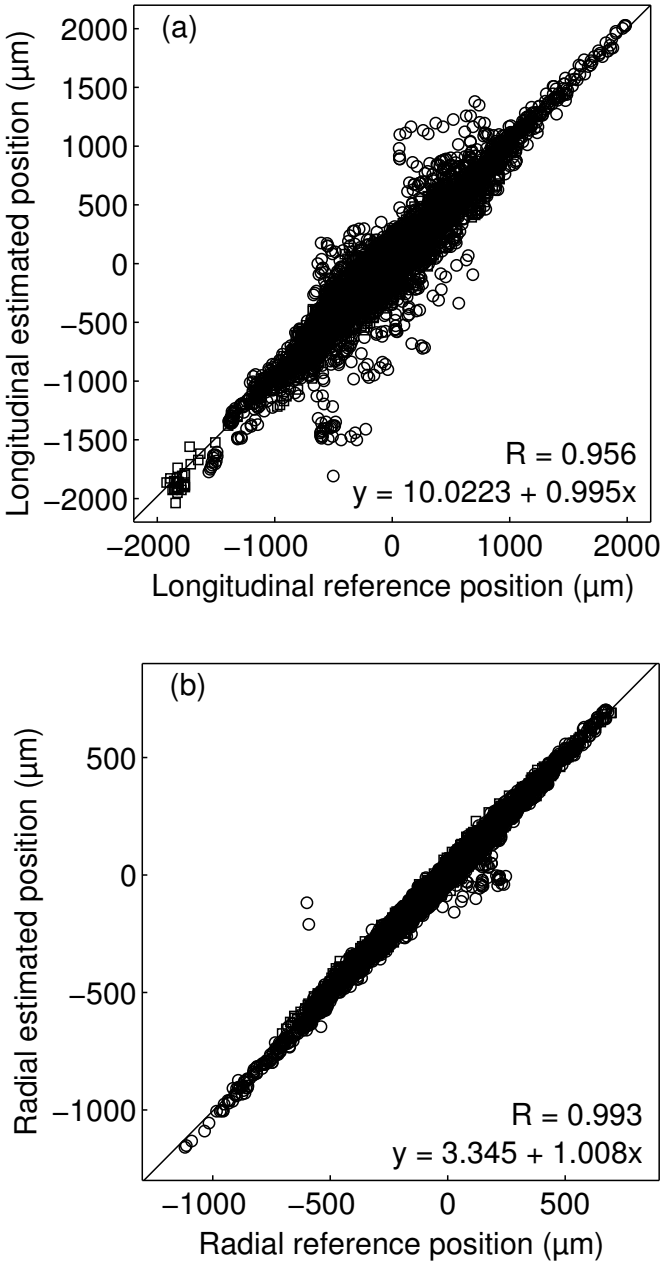

Figure 9: Linear regression line and correlation coefficient R between the reference position of the tracked point $\mathbf{p}$ and its estimation performed by our KBM method, during the whole length of each sequence, for healthy volunteers (circles) and at-risk patients (squares), in the longitudinal (a) and radial (b) directions. For each sequence, the zero coordinate corresponds to the position of the point in the first frame.

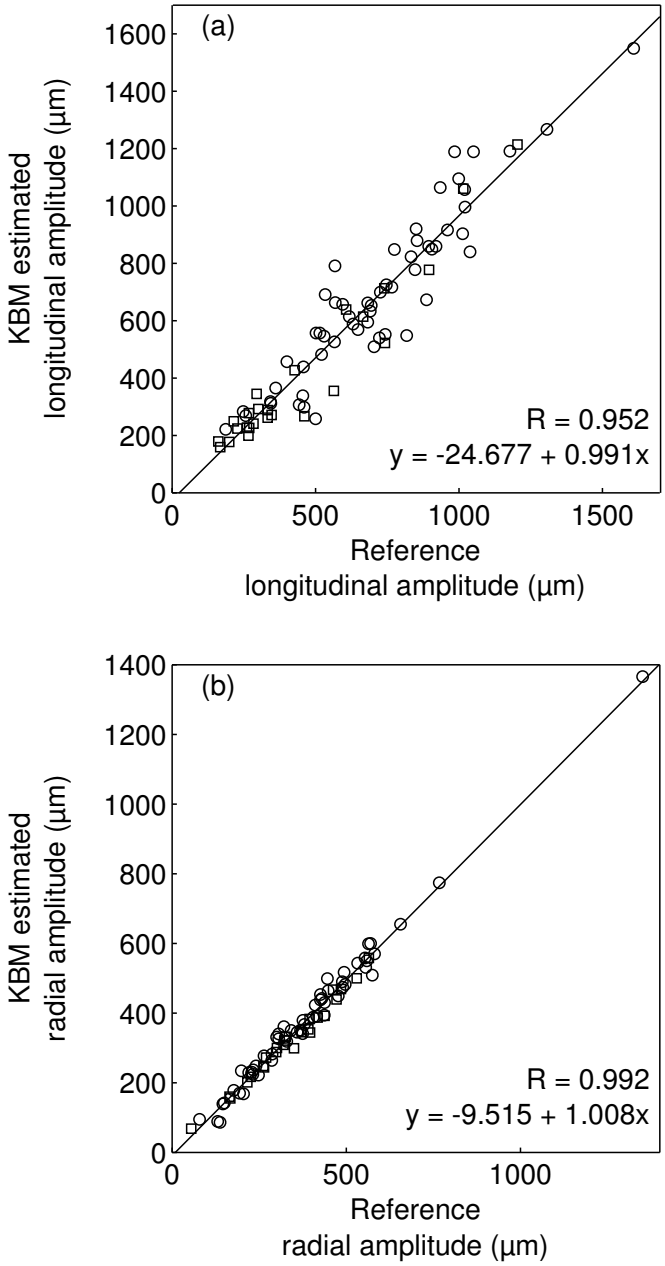

Figure 10: Linear regression line and correlation coefficient R between the reference value of the motion amplitude and the estimation performed by our KBM method, for healthy volunteers (circles) and at-risk patients (squares), in the longitudinal (ΔX, a) and radial (ΔY, b) directions.

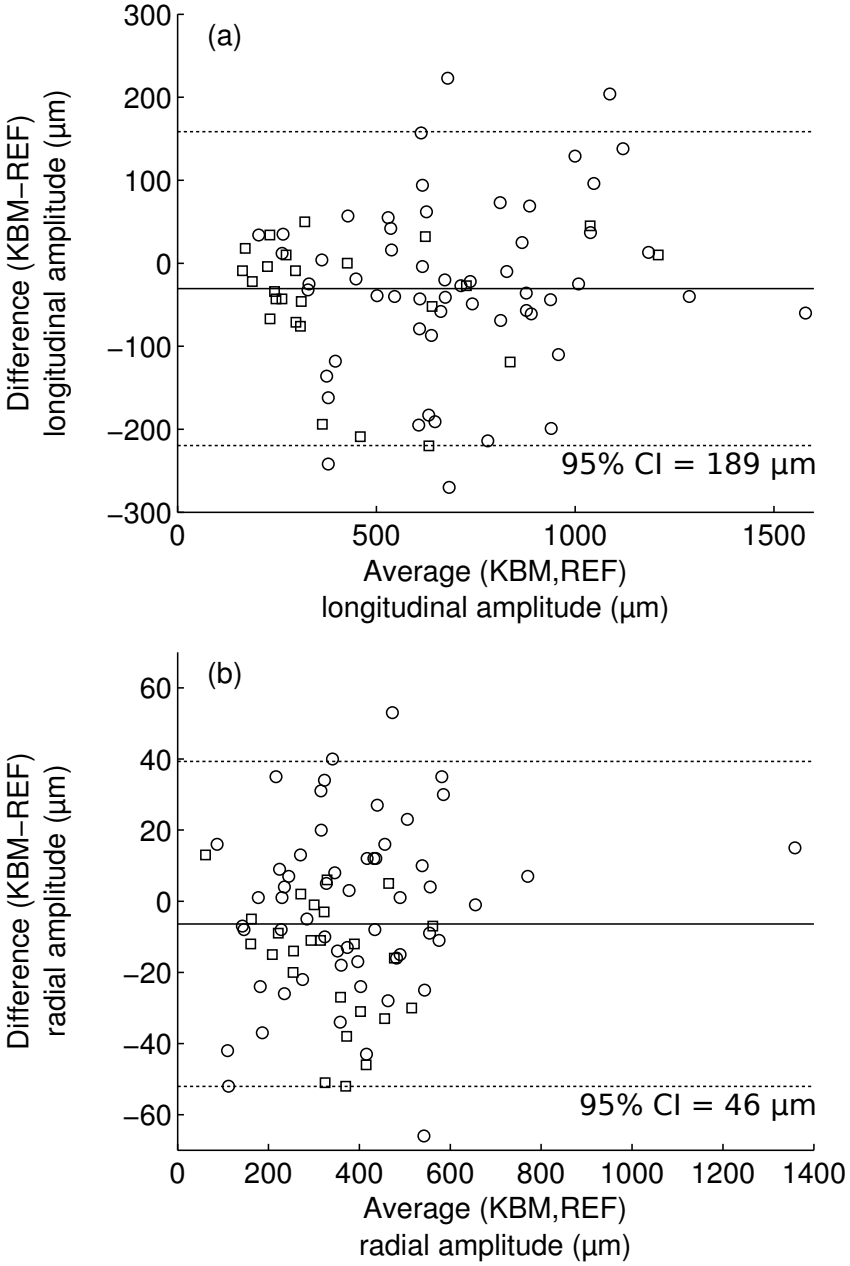

Figure 11: Bland-Altman plot comparing the motion amplitude estimated by our KBM method with the reference (REF), for healthy volunteers (circles) and at-risk patients (squares), in the longitudinal (ΔX, a) and radial (ΔY, b) direction.

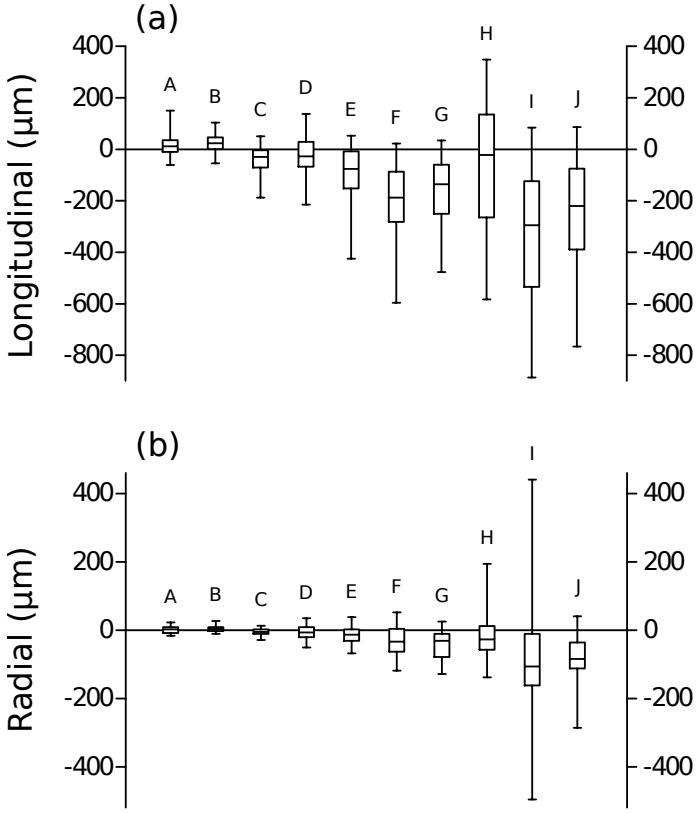

Figure 12: Box plot representing the dispersion of the estimated motion amplitude from the reference (zero level), in the longitudinal (ΔX, a) and radial (ΔY, b) directions, for the three observers O_1, O_2, and O_3 (A-C), KBM (D), KBM$_{bis}$ (E), MBM (F), BM (G), BM$_{bis}$ (H), BM$_{ter}$ (I), and VVI (J). Percentiles are indicated by boxes (25^{th} and 75^{th}), inner lines (50^{th}) and error bars (5^{th} and 95^{th}).

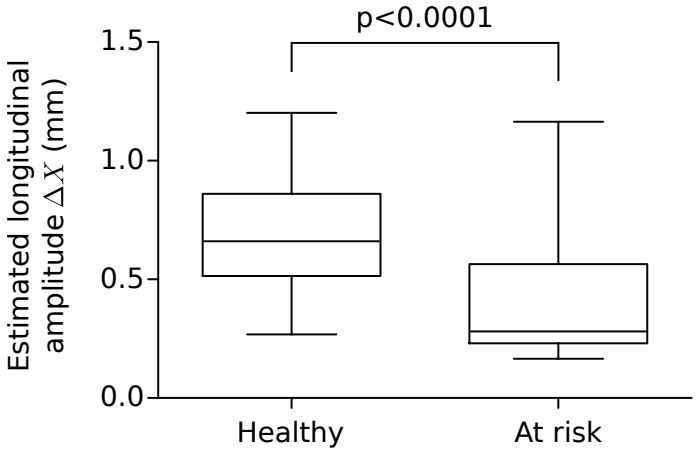

Figure 13: Box plot representing the longitudinal motion amplitude, for healthy volunteers and at-risk patients. Percentiles are indicated by boxes (25^{th} and 75^{th}), inner lines (50^{th}) and error bars (5^{th} and 95^{th}). The result of the Mann–Whitney U test is indicated by the p value.

Tables

Table 1: Parameter settings for the different block matching methods

Method	Size: longitudinal × radial		
	Block	Window	Margin
KBM, KBM_{bis}, BM	$1.50 \times 0.30\,\text{mm}^2$	$2.50 \times 1.30\,\text{mm}^2$	$[0.50,\ 0.50]$ mm
MBM	$1.50 \times 0.30\,\text{mm}^2$	$2.50 \times 0.70\,\text{mm}^2$	$[0.50,\ 0.20]$ mm
BM_{bis}	$0.10 \times 0.10\,\text{mm}^2$	$0.70 \times 0.70\,\text{mm}^2$	$[0.30,\ 0.30]$ mm
BM_{ter}	$3.20 \times 2.50\,\text{mm}^2$	$4.50 \times 3.80\,\text{mm}^2$	$[0.65,\ 0.65]$ mm

Table 2: Tracking absolute errors in μm

Method	Longitudinal	Radial
	Healthy (n=56)	
KBM *vs* Reference	89 ± 117	20 ± 20
KBM_{bis} *vs* Reference	170 ± 185	58 ± 62
BM *vs* Reference	235 ± 239	111 ± 111
BM_{bis} *vs* Reference	592 ± 569	194 ± 304
BM_{ter} *vs* Reference	223 ± 202	102 ± 113
MBM *vs* Reference	174 ± 177	46 ± 49
Inter-observers variability	97 ± 142	25 ± 30
Intra-observer variability	71 ± 125	15 ± 19
	At-risk (n=25)	
KBM *vs* Reference	69 ± 72	20 ± 16
KBM_{bis} *vs* Reference	111 ± 146	63 ± 52
BM *vs* Reference	160 ± 156	142 ± 129
BM_{bis} *vs* Reference	307 ± 278	195 ± 272
BM_{ter} *vs* Reference	175 ± 152	124 ± 121
MBM *vs* Reference	125 ± 115	42 ± 35
Inter-observers variability	59 ± 51	23 ± 20
Intra-observer variability	32 ± 26	10 ± 8
	All (n=81)	
KBM *vs* Reference	84 ± 107	20 ± 19
KBM_{bis} *vs* Reference	154 ± 177	59 ± 60
BM *vs* Reference	215 ± 222	120 ± 117
BM_{bis} *vs* Reference	515 ± 523	194 ± 296
BM_{ter} *vs* Reference	210 ± 191	108 ± 116
MBM *vs* Reference	161 ± 164	45 ± 45
Inter-observers variability	87 ± 125	24 ± 28
Intra-observer variability	60 ± 109	13 ± 17

Table 3: Peak-to-peak amplitude absolute errors in μm

Method	Longitudinal	Radial
	Healthy (n=56)	
KBM *vs* Reference	82 ± 70	19 ± 15
KBM_{bis} *vs* Reference	141 ± 134	26 ± 22
BM *vs* Reference	208 ± 146	47 ± 39
BM_{bis} *vs* Reference	249 ± 219	64 ± 76
BM_{ter} *vs* Reference	391 ± 213	79 ± 41
MBM *vs* Reference	262 ± 183	53 ± 41
VVI *vs* Reference	263 ± 207	95 ± 76
VVI variability	128 ± 117	40 ± 48
Inter-observers variability	95 ± 118	16 ± 17
Intra-observers variability	79 ± 119	21 ± 22
	At risk (n=25)	
KBM *vs* Reference	58 ± 63	19 ± 15
KBM_{bis} *vs* Reference	69 ± 88	22 ± 20
BM *vs* Reference	116 ± 121	53 ± 48
BM_{bis} *vs* Reference	179 ± 109	67 ± 73
BM_{ter} *vs* Reference	194 ± 144	100 ± 54
MBM *vs* Reference	130 ± 132	41 ± 30
Inter-observers variability	43 ± 34	17 ± 15
Intra-observer variability	25 ± 25	8 ± 7
	All (n=81)	
KBM *vs* Reference	74 ± 68	19 ± 15
KBM_{bis} *vs* Reference	118 ± 125	25 ± 21
BM *vs* Reference	180 ± 144	49 ± 42
BM_{bis} *vs* Reference	228 ± 194	65 ± 75
BM_{ter} *vs* Reference	330 ± 212	85 ± 46
MBM *vs* Reference	221 ± 179	49 ± 38
Inter-observers variability	79 ± 103	16 ± 16
Intra-observer variability	62 ± 103	17 ± 19

References

Ahlgren, Å., Cinthio, M., Steen, S., Nilsson, T., Sjöberg, T., Persson, H., Lindström, K., 2012. Longitudinal displacement and intramural shear strain of the porcine carotid artery undergo profound changes in response to catecholamines. American Journal of Physiology - Heart and Circulatory Physiology 302, H1102–H1115.

Ahlgren, Å., Cinthio, M., Steen, S., Persson, H., Sjöberg, T., Lindström, K., 2009. Effects of adrenaline on longitudinal arterial wall movements and resulting intramural shear strain: a first report. Clinical Physiology and Functional Imaging 29, 353–359.

Bohs, L., Trahey, G., 1991. A novel method for angle independent ultrasonic imaging of blood flow and tissue motion. IEEE Transactions on Biomedical Engineering 38, 280–286.

Cinthio, M., Ahlgren, Å., Bergkvist, J., Jansson, T., Persson, H., Lindström, K., 2006. Longitudinal movements and resulting shear strain of the arterial wall. American Journal of Physiology 291, H394–H402.

Cinthio, M., Ahlgren, Å., Jansson, T., Eriksson, A., Persson, H., Lindström, K., 2005. Evaluation of an ultrasonic echo-tracking method for measurements of arterial wall movements in two dimensions. IEEE Transactions on Ultrasonics, Ferroelectrics, and Frequency Control 52, 1300–1311.

Ford, E., 2005. Risks for all-cause mortality, cardiovascular disease, and diabetes associated with the metabolic syndrome: a summary of the evidence. Diabetes care 28, 1769–1778.

Gamble, G., Zorn, J., Sanders, G., MacMahon, S., Sharpe, N., 1994. Estimation of arterial stiffness, compliance, and distensibility from M-mode ultrasound measurements of the common carotid artery. Stroke 25, 11–16.

Gastounioti, A., Golemati, S., Stoitsis, J., Nikita, K., 2011. Comparison of kalman-filter-based approaches for block matching in arterial wall motion analysis from B-mode ultrasound. Measurement Science and Technology 22, 114008.1–114008.9.

Golemati, S., Sassano, A., Lever, M., Bharath, A., Dhanjil, S., Nicolaides, A., 2003. Carotid artery wall motion estimated from B-mode ultrasound using region tracking and block matching. Ultrasound in Medecine & Biology 29, 387–399.

Kalman, R., 1960. A new approach to linear filtering and prediction problems. Transactions of theASME – Journal of Basic Engineering 82D, 35–45.

Laurent, S., Boutouyrie, P., Asmar, R., Gautier, I., Laloux, B., Guize, L., Ducimetiere, P., Benetos, A., 2001. Aortic stiffness is an independent predictor of all-cause and cardiovascular mortality in hypertensive patients. Hypertension 37, 1236–1241.

Mutlu, B., Tigen, K., Gurel, E., Ozben, B., Karaahmet, T., Basaran, Y., 2011. The predictive value of flow-mediated dilation and carotid artery intima-media thickness for occult coronary artery disease. Echocardiography 28, 1141–1147.

Ophir, J., Cespedes, I., Ponnekanti, H., Yazdi, Y., Li, X., 1991. Elastography: a quantitative method for imaging the elasticity of biological tissues. Ultrasonic imaging 13, 111–134.

Persson, M., Ahlgren, Å., Jansson, T., Eriksson, A., Persson, H., Lindström, K., 2003. A new non-invasive ultrasonic method for simultaneous measurements of longitudinal and radial arterial wall movements: first in vivo trial. Clinical Physiology and Functional Imaging 23, 247–251.

Simon, A., Chironi, G., Levenson, J., 2006. Performance of subclinical arterial disease detection as a screening test for coronary heart disease. Hypertension 48, 392–396.

Simons, P., Algra, A., Bots, M., Grobbee, D., van der Graaf, Y., 1999. Common carotid intima-media thickness and arterial stiffness: Indicators of cardiovascular risk in high-risk patients – the smart study (second manifestations of arterial disease). Circulation 100, 951–957.

Svedlund, S., Eklund, C., Robertsson, P., Lomsky, M., Gan, L., 2011. Carotid artery longitudinal displacement predicts 1-year cardiovascular outcome in patients with suspected coronary artery disease. Arteriosclerosis, Thrombosis, and Vascular Biology 31, 1668–1674.

Svedlund, S., Gan, L., 2011. Longitudinal wall motion of the common carotid artery can be assessed by velocity vector imaging. Clinical Physiology and Functional Imaging 31, 32–38.

Welch, G., Bishop, G., 1995. An introduction to the kalman filter. University of North Carolina, Department of Computer Science, TR 95-041 .

WHO, 2011. World health statistics report, World Health Organisation.

771 Zahnd, G., Boussel, L., Marion, A., Durand, M., Moulin, P., Sérusclat, A., Vray,
772 D., 2011a. Measurement of two-dimensional movement parameters of the carotid
773 artery wall for early detection of arteriosclerosis: a preliminary clinical study.
774 Ultrasound in Medecine & Biology 37, 1421–1429.

775 Zahnd, G., Boussel, L., Sérusclat, A., Vray, D., 2011b. Intramural shear strain can
776 highlight the presence of atherosclerosis: a clinical in vivo study. IEEE Ultrasonics
777 Symposium, Orlando, Florida (USA) , 1770–1773.

778 Zahnd, G., Vray, D., Sérusclat, A., Alibay, D., Bartold, M., Brown, A., Durand,
779 M., Jamieson, L., Kapellas, K., Maple-Brown, L., O'Dea, K., Moulin, P., Celer-
780 majer, D., Skilton, M., 2012. Longitudinal displacement of the carotid wall and
781 cardiovascular risk factors: associations with aging, adiposity, blood pressure and
782 periodontal disease independent of cross-sectional distensibility and intima-media
783 thickness. Ultrasound in Medecine & Biology 38, 1705–1715.